Eur. Phys. J. D **4**, 31–38 (1998)

THE EUROPEAN PHYSICAL JOURNAL D

Resonant widths, line intensities and lineshapes for MQDT models with two or more open channels

S. Cohen[a]

Institute of Accelerating Systems and Applications, P.O. Box 17214, 10024 Athens, Greece

Received: 26 May 1998 / Accepted: 1st July 1998

Abstract. Approximate analytical formulae describing the energy variation of line intensities, autoionization widths and lineshape asymmetries, are derived for a Phase-Shifted Multichannel Quantum Defect Theory model composed of two closed interacting channels coupled to two effective continua. This is accomplished by putting the two compatibility equation solutions, for the common phase shifts of the two open channels, in such a form so the resonant behavior is attributed to one of them, the other accounting for an energy dependent background. Then, the well-known procedures for the simpler case where only one continuum is considered are applied, using only the resonant solution. The method is quite general and applicable to any MQDT model with two or more open channels. The resulting analytical formulae are tested on experimental spectra of Sr, Ba and Cu and it is shown that they are valid as long as: i) The resonances are non-overlapping, ii) The direct closed channel coupling is much stronger than the indirect one through the continua and (when excitation matrix elements are involved) iii) The open channels excitation strength is smaller or at least comparable to the closed channels one.

PACS. 32.80.Dz Autoionization – 32.80.Rm Multiphoton ionization and excitation to highly excited states (e.g., Rydberg states) – 32.80.Fb Photoionization of atoms and ions

1 Introduction

The Multichannel Quantum Defect Theory (MQDT) [1] is a powerful tool for the analysis of atomic spectra. The configuration interaction between Rydberg series (closed channels) converging towards different ionization limits as well as their coupling to the available continua (open channels) can be described in a unified and compact manner, using a relatively small set of parameters. If the number of interacting channels is large these parameters are provided by the R-matrix method [2], able to calculate the channel interactions inside the ionic core seen by the excited Rydberg electron. When however the number of channels is small, the parameters may be fitted to the experimental spectra. Restricting ourselves to this latter case, widely used nowadays is the phase-shifted MQDT [3,4] where we have to deal with two basic types of parameters which may be interpreted as channel couplings and quantum defects of unperturbed channels. In many cases the number of open channels is quite high but as discussed by several authors [4–6] all the features of the total cross-section (apart from a constant background) may be reproduced by including only a reduced number of effective continua. Using his complex reaction matrix MQDT formalism, Lecomte [6] treated this concept in more detail and established the rules to be followed for its application. The number of effective continua should be equal to the number of closed channels and the first closed channel should be coupled to the first continuum, the second to two continua (including the first one) and so on. Additionally, the continua may be considered uncoupled. An MQDT model constructed under those rules can be characterized as "complete" in order to be distinguished from a rigorous theory including all relevant interacting channels. In practice many simplifications are usually made, in order to keep the number of fitted parameters reasonable and to obtain semi- analytical MQDT solutions. One model which can be solved analytically consists of two interacting closed channels converging towards different ionization limits and coupled to the same continuum. Treated in detail in the past [4,7–10], this model (called 3QDT hereafter) has been often used to fit the so-called complex resonances [7,11,12] where a perturber is diluted in a large number of a perturbed series members. The spectral features of a complex resonance are sometimes spectacular. The most well-known effects are the reversed line asymmetry (q-reversal) [13] and the inhibited autoionization (stabilization) [14] associated with quasi-zero autoionization widths. The extensive use of 3QDT, even in situations where it is clearly not "complete", is to a large extend due to its pedagogical character. It provides fairly simple analytical expressions for the energy dependence of the widths, line intensities and Fano parameter q near a complex resonance,

[a] e-mail: cohens@rtm.iasa.uoa.gr

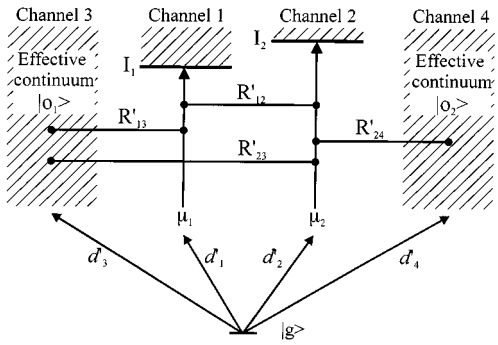

Fig. 1. Schematic diagram of the Phase-Shifted 4QDT model. For the parameters shown see text.

offering this way insight into the mechanisms producing the above mentioned phenomena. On the other hand, although the conditions of validity of these expressions have been previously discussed [7–10] they have not been fully explored using specific examples from existing experimental spectra. Even more, such analytical expressions do not exist for models with more than one open channels. The main purpose of this paper is to derive the corresponding formulae for 4QDT *i.e.* for a "complete" model consisting of two interacting closed channels converging towards different ionization limits and coupled to two effective continua. Thus, the previous work on 3QDT [4–7] is extended while preserving the same level of simplicity and insight. This is accomplished by first effectively reducing the problem to a single-open-channel one and then applying the procedures already employed for 3QDT. It is furthermore shown that the method can be generalized for models with more complicated closed channel systems and an arbitrary number of continua. Finally, the 4QDT expressions are tested and their conditions of applicability are examined using the preliminary experimental results on the $[5pnp]_{J=0}$ spectrum of Sr [15], the $[6pnd]_{J=3}$ spectrum of Ba [11] and the Cu $3d^9 4s(^1D_2)nd^2G_{9/2}$ series interacting with the $3d^9 4p^2\ ^4\mathrm{F}_{9/2}$ perturber [16].

2 Two-open-channel MQDT and the 4QDT model

2.1 Standard elements of MQDT

In the following, emphasis is given on models having two continua while the system of closed channels is left unspecified. However, many important details can be better understood by using the specific example of the 4QDT model to which our formal approximate expressions will be finally applied. This is shown in Figure 1 and it is a simplified version of the one presented in reference [16] where all the possible couplings between open and closed channels were included. Some of the couplings are eliminated in the model of Figure 1. Nevertheless it is "complete" in the sense given in the introduction. Provided all relevant closed channels are considered, it is able to reproduce all the features of the spectrum apart from a constant background while all MQDT parameters are constant or smooth functions of energy. It consists of two coupled closed channels 1 and 2 converging to the different ionization limits I_1 and I_2 ($I_2 > I_1$). It also includes two uncoupled effective continua $|o_1\rangle$ and $|o_2\rangle$ (open channels 3 and 4 respectively). Channel 1 may autoionize only to $|o_1\rangle$ while channel 2 to both open channels. The basic matrix MQDT equation to be solved is given by

$$[\mathbf{R}' + \mathbf{T}]\mathbf{a} = \mathbf{0}. \tag{1}$$

The phase-shifted reaction matrix $\mathbf{R}'$ has zero diagonal elements while its off-diagonal ones account for the coupling between all the channels. The elements of the diagonal matrix $\mathbf{T}$ are given by $T_i = \tan(\pi\nu_i')$ with $\nu_i' = \nu_i + \mu_i$. The parameters μ_i may be interpreted as the zero-coupling quantum defects of each channel *i.e.* when $\mathbf{R}' = \mathbf{0}$. The $\mathbf{a}$ vector is related to the vector $\mathbf{Z}$ of the channel admixture coefficients by $a_i = Z_i \cos(\pi\nu_i')$. The compatibility condition for (1) to have a non-trivial solution is

$$\det[\mathbf{R}' + \mathbf{T}] = 0. \tag{2}$$

Let us, in a first step, ignore the open channels. Using the well-known partitioning in four quadrants [1,4]

$$[\mathbf{R}' + \mathbf{T}] = \begin{bmatrix} [\mathbf{R}' + \mathbf{T}]_{cc} & \mathbf{R}'_{co} \\ \mathbf{R}'_{oc} & [\mathbf{R}' + \mathbf{T}]_{oo} \end{bmatrix} \tag{3}$$

(the subscript "o" stands for open and "c" for closed) and denoting by D_{cc} the determinant of (2) for this reduced problem, the energy level positions are determined by satisfying simultaneously the equation

$$D_{cc} \equiv \det\Big[[\mathbf{R}' + \mathbf{T}]_{cc}\Big] = 0 \tag{4}$$

and the relations

$$I_i - Ryd/\nu_i^2 = I_j - Ryd/\nu_j^2,\ i \neq j \tag{5}$$

between the effective quantum numbers defined with respect to each ionization limit of the closed channel system (Ryd is the mass corrected Rydberg constant). Then a fitting of the predicted values to the experimental energy levels determines the unperturbed quantum defects and provides information for the coupling parameters between the closed channels. For the 4QDT model the determined parameters are μ_1, μ_2 and $|R'_{12}|$. The quality of the fit is assessed by inspection of graphical representations of equation (4) (Lu-Fano curves [17]) in terms of plots of ν_i *versus* ν_j.

Now, introducing in a second step the open channels, the photoionization cross-section from an initial valence (non-Rydberg) level $|g\rangle$ is written as

$$\sigma(E) \propto \sum_{\rho=1}^{n_o} \left[\sum_{i=1}^{N} a_i^{(\rho)} d_i'\right]^2 \tag{6}$$

where d_i' is the dipole matrix element between $|g\rangle$ and the channel $|i\rangle$ and N is the total number of channels. The index ρ in (6) runs over the number n_o of

open channels (here $n_o = 2$) which is the number of independent solutions of (1). For each solution we require a common phase shift $\delta^{(\rho)}$ for the open channels so $\tan(\pi\nu'_{o_1}) = \tan(\pi\nu'_{o_2}) = \tan(-\delta^{(\rho)}) \equiv \epsilon_\rho$. The solution of (2) provides ϵ_ρ for $\rho = 1, 2$ and the coefficients $a_i^{(\rho)}$ are then determined by (1) and the normalization condition $\left(a_{o_1}^{(\rho)}\right)^2 + \left(a_{o_2}^{(\rho)}\right)^2 = \left(1+\epsilon_\rho^2\right)^{-1}$.

2.2 Formal derivation of approximate width, line intensity and lineshape expressions

As long as an MQDT model is "complete" and includes all relevant closed channels, (6) may reproduce the spectrum irrespectively of its complexity. On the other hand, it is not always possible, even for a small number of interacting channels, to describe through semi-analytical formulae the behavior of quantities such as widths and lineshapes in the neighborhood of a complex resonance. In 3QDT this became feasible only after assuming the validity of two conditions:

(i) The resonances are non-overlapping. In other words the widths of successive members of Rydberg series, if considered unperturbed, are smaller than their separation. This implies that $\left(R'_{io_j}\right)^2 < 1$ [3,6,18], where R'_{io_j} couples the closed channel $|i\rangle$ with the open channel $|o_j\rangle$. In this case the resonant behavior is associated with the poles of $\tan(-\delta^{(\rho)})$ *i.e.* with $\epsilon_\rho \to \infty$.

(ii) If, furthermore, the direct closed channel coupling is stronger than the indirect one through the continua, the resonances are located very close to the energy level positions predicted by (4) [7]. Stated in another way, to a very good approximation $D_{cc} = 0$ presumes $\epsilon_\rho \to \infty$. Especially for the 3QDT and 4QDT models, R'_{12} is responsible for the direct coupling while the indirect is characterized by the product $R'_{13}R'_{23}$. A quantitative criterion for the dominance of the former could be the requirement that $|R'_{12}/R'_{13}R'_{23}| \gg 1$.

The above conditions (i) and (ii) are a necessary ingredient of the following analysis and they will be assumed hereafter to be valid. One should note however that a definite answer concerning the validity of (i) can only be given by a nearly *ab initio* R-matrix/MQDT treatment. Even when (i) is invalid, a fitting procedure may lead to a set of parameters fulfilling this condition.

For any model with two open channels, (2) reduces to the quadratic equation

$$D_{cc}\epsilon_\rho^2 - B\epsilon_\rho + C = 0. \tag{7}$$

It is, of course, trivial to solve (7). Using the standard forms of the two solutions, it is easy to verify that resonant behavior, $\epsilon_\rho \to \infty$, is exhibited by both roots (since both are proportional to D_{cc}^{-1}) but not simultaneously. However, it would be desirable to somehow attribute this behavior to only one of them. Indeed, this can be achieved by writing the solutions in the form

$$\epsilon_{res} = \frac{A}{D_{cc}} \tag{8a}$$

and

$$\epsilon_{nr} = \frac{C}{A} \tag{8b}$$

where

$$A = \frac{1}{2}(B + \mathrm{Sign}(B)\sqrt{B^2 - 4D_{cc}C}). \tag{8c}$$

Equations (8a–c) are known to be the most trouble-free forms that the solutions of (7) can be put in for computational purposes [19]. Of interest here however, is the resulting unequal partitioning of the resonant features which are now exhibited only by the root ϵ_{res} while the non-resonant root ϵ_{nr} accounts just for an energy dependent continuum structure. It is only for $C|_{D_{cc}=0} \to \infty$ or $B|_{D_{cc}=0} \approx 0$, that ϵ_{nr} may show resonant behavior. These conditions are not met, except may be accidentally as a result of an oversimplification of the model (for example, by unreasonably minimizing the number of fitted parameters) and these poles do not correspond to true energy levels.

Adopting (8a–c) leads very easily to the derivation of the width function $\Gamma(E)$. We start from the general formula [10,18]

$$\Gamma(E) = 4Ryd\left[\frac{\partial\delta}{\partial E}\Big|_{E=E_r}\right]^{-1} \tag{9}$$

for an isolated resonance located at E_r. The condition $E = E_r$ is replaced now by (4) and setting $\epsilon_{res} = \tan(-\delta)$ (while ϵ_{nr} is discarded) we arrive at

$$\Gamma(E) = 4Ryd\left[\frac{\partial D_{cc}}{\partial E}\Big|_{D_{cc}=0}\right]^{-1} B|_{D_{cc}=0}. \tag{10}$$

The $\sigma_{max}(E)$ function may be found by setting $D_{cc} = 0$ in (6)

$$\sigma_{max}(E) = \sigma(E)|_{D_{cc}=0} = \sigma_{max}^{res}(E) + \sigma_{max}^{nr}(E). \tag{11}$$

It turns out that $\sigma_{max}^{res}(E)$ depends only on the matrix elements describing excitation to the closed channels while $\sigma_{max}^{nr}(E)$ depends generally on all matrix elements. This second non-resonant term is absent in 3QDT. However, the corresponding 3QDT expression for $\sigma_{max}(E)$ [7], similarly to $\sigma_{max}^{res}(E)$, does not depend on the continuum matrix element. An additional necessary condition, apart from (i) and (ii), for the 3QDT $\sigma_{max}(E)$ function to be meaningful, and which has not been pointed out previously, is that:

(iii) The continuum matrix elements are of weaker or at least similar magnitude compared to the closed channel ones.

To get a feeling about the significance of (iii), assume that all the closed channel matrix elements are zero. Then, $\sigma_{max}(E)$ for 3QDT and $\sigma_{max}^{res}(E)$ in (11) are identically zero and the spectrum is dominated by window resonances. Consequently, these two functions describe the profile of resonant excitation only, except when (iii) is valid, in which case they describe the total cross-section envelope and we may write

$$\sigma_{max}(E) \approx \sigma_{max}^{res}(E). \tag{12}$$

The third quantity of interest for the analysis of the spectra is the energy dependent Fano parameter $q(E)$. The procedure which is generally followed for its calculation is to first rearrange the cross-section in a form suggestive of a Fano profile for an isolated resonance, $\sigma(E) = \sigma_b + \sigma_a(x+q)^2/(x^2+1)$, and then try to identify x and q. Several methods have been proposed to accomplish that [10,20,21]. Here, we adopt the method of reference [10] leading to a simple and easily interpretable formula for $q(E)$. The energy variable x is defined at the outset as $x = 1/\epsilon_{res}$. The part of the total cross-section corresponding to ϵ_{nr} may be identified in our case as an energy-dependent background σ_b. Bringing the remaining resonant part to the desired functional form results in an energy-dependent σ_a and to a Fano parameter q which rapidly oscillates with energy. To obtain a physically meaningful parameter, q is evaluated on the resonance positions by again setting $D_{cc} = 0$.

2.3 Application to 4QDT

For the model of Figure 1 the functions D_{cc}, B and C are given by

$$D_{cc} = T_1T_2 - R_{12}'^2 \tag{13a}$$

$$B = T_2R_{13}'^2 + T_1\left[R_{23}'^2 + R_{24}'^2\right] - 2R_{12}'R_{13}'R_{23}' \tag{13b}$$

$$C = R_{13}'^2R_{24}'^2. \tag{13c}$$

Inserting (13a–c) to (10) and (12) the $\Gamma(E)$ function, assuming energy-independent parameters, is written as

$$\Gamma(E) = \frac{4Ryd}{\pi}\frac{R_{12}'^2R_{24}'^2 + [R_{12}'R_{23}' - T_2R_{13}']^2}{\nu_1^3[R_{12}'^4 + T_2^2] + \nu_2^3[1+T_2^2]R_{12}'^2} \tag{14}$$

while the $\sigma_{max}(E)$ function is given by

$$\sigma_{max}(E) \propto \frac{[T_2d_1' - R_{12}'d_2']^2}{R_{12}'^2R_{24}'^2 + [R_{12}'R_{23}' - T_2R_{13}']^2}\,. \tag{15}$$

It can be observed that the denominator of $\sigma_{max}(E)$ in (15) is found in the numerator of $\Gamma(E)$ in (14). This is a common feature with 3QDT. In the latter case this fact characterizes the stabilization effect ($\Gamma = 0,\ \sigma_{max}(E) \to \infty$), occurring when for a level position the equation $R_{12}'R_{23}' - T_2R_{13}' = 0$ is fulfilled. This exact stabilization is avoided in 4QDT due to the existence of the coupling parameter R_{24}' representing an autoionization decay to the second continuum, destroying in this way the interference underlying the effect. Nevertheless, approximate stabilization can occur if R_{24}' is small. Lecomte [6] arrived at the same conclusions using a model similar to 4QDT. He also presented an approximate formula which resembles (14) in the limit $\nu_1 \gg \nu_2$.

Following the procedure outlined in the previous subsection we find that $q(E)$ is given by

$$q(E) = -\frac{T_2d_1' - R_{12}'d_2'}{R_{12}'R_{24}'d_4' + (R_{12}'R_{23}' - T_2R_{13}')d_3'} \tag{16}$$

which predicts two q-reversals. The first one is located at $T_2 = R_{12}'d_2'/d_1'$ where $q(E)$ passes smoothly from zero. At exactly this same location (15) becomes zero implying a vanishing resonant excitation and confirming the above made comments about $\sigma_{max}(E)$. The second q-reversal occurs when the denominator of (16) becomes zero and $q(E)$ has a pole. Wang and Greene [21] pointed out that there may be more than one poles of $q(E)$ which (16) does not predict. A more rigorous treatment would require the application of their method which is however of little inspectional usefulness since it does not lead to simple analytical results.

2.4 4QDT expressions applicable to isolated core excitation

It is worth mentioning another approach for the calculation of an energy-dependent asymmetry parameter. For 3QDT, Cooke and Cromer [4] rearranged only the admixture coefficient Z_2^2 assuming excitation of channel 2 (the perturbers) alone through the Isolated Core Excitation (ICE) method [22]. The latter has been used mainly in Alkaline Earth atoms having two valence electrons and in this case the initial state $|g\rangle$ is a Rydberg one. The absorption spectrum is much simpler, its main feature being the suppression of continuum excitation. As a consequence, in ICE (16) is meaningless. For the sake of completeness we provide the set of 4QDT formulae appropriate for the ICE method. The cross-section considering excitation of channel 2 only is written as

$$\sigma^{ICE}(E) \propto \nu_2^3O^2(n^*,\ \nu_2)\Big[(Z_2^{res})^2 + (Z_2^{nr})^2\Big] \tag{17}$$

where $O(n^*,\ \nu_2) = 2(n^*\nu_2)^{1/2}[\pi(n^{*2} - \nu_2^2)]^{-1}\ \sin[\pi(n^* - \nu_2)]$, is the overlap integral between the initial and final state of the Rydberg electron [22] (n^* is the effective quantum number of the initial Rydberg state). Since ICE probes only the closed channel 2 character of the final wavefunction, while the continuum is not excited, it is an excellent approximation to assume that $(Z_2^{res})^2 \gg (Z_2^{nr})^2$. The spectral characteristics are determined almost solely from $(Z_2^{res})^2$ which can be put in the form

$$(Z_2^{res})^2 = \frac{[R_{23}'^2 + R_{24}'^2](1+T_2^2)}{T_2^2 + [R_{23}'^2 + R_{24}'^2]^2}\frac{\left(T_1 - s + \gamma q^{ICE}\right)^2}{(T_1-s)^2 + \gamma^2}\,. \tag{18}$$

The first factor in (18) corresponds to the quasi-symmetric profile of the character of channel 2 in the absence of any coupling. This profile is modulated by the second factor containing the functions γ, s and q^{ICE}, interpreted as shift, width and asymmetry parameter respectively of the perturbed series resulting from the coupling with the perturber. They are given by

$$\gamma(E) = \frac{R'^2_{12}R'^2_{24} + [R'_{12}R'_{23} - T_2R'_{13}]^2}{T_2^2 + [R'^2_{23} + R'^2_{24}]^2} \tag{19}$$

$$s(E) = \frac{T_2\Big[R'^2_{12} - R'^2_{13}[R'^2_{23} + R'^2_{24}]\Big] + 2R'_{12}R'_{13}R'_{23}[R'^2_{23} + R'^2_{24}]}{T_2^2 + [R'^2_{23} + R'^2_{24}]^2} \tag{20}$$

$$q^{ICE}(E) = -\frac{1}{\gamma(E)}\Bigg\{ - s(E) + \frac{R'^2_{12}}{T_2}\Bigg[1 - \Bigg(\frac{R'^2_{12}R'^2_{24} + [R'_{12}R'_{23} - T_2R'_{13}]^2}{R'^2_{12}[R'^2_{23} + R'^2_{24}]}\Bigg)^{1/2}\Bigg]\Bigg\}. \tag{21}$$

The formulae (19, 20, 21) probe internal atomic interferences irrespectively of the excitation process [6,14]. Therefore, and as is the case also for (14), they do not depend on the validity of (iii). However, $\gamma(E)$ and $s(E)$ must be regarded as qualitative quantities rather than true widths and shifts. Especially for the resonant widths, it is (14) which should be used to fit the experimental data, not (19). The function $q^{ICE}(E)$ on the other hand, is the asymmetry parameter appropriate for the ICE method while (16) is appropriate when excitation takes place from a valence state.

The expressions (14, 15, 16) as well as (19, 20, 21) are the extensions of the corresponding ones for 3QDT to which they reduce for $R'_{24} = 0$ and $d'_4 = 0$.

3 Generalization to arbitrary number of open channels

For a model having n_o open channels the compatibility equation (2) acquires the following polynomial form:

$$D_{cc}\epsilon^{n_o} - B\epsilon^{n_o-1} + \cdots = 0. \tag{22}$$

By applying the ideas presented in Section 2.2 to successive pairs of roots of (22), the resonant behavior can always be attributed to only one root. This root is given by an expression identical to (8a). The function A is very complicated but it needs to be calculated only on the resonant positions satisfying (4), in which case it turns out that $A|_{D_{cc}=0} = B|_{D_{cc}=0}$. Finally, the function B, which is given by the sum of the n_o roots of (22) multiplied by D_{cc}, is expressed as

$$B = D_{cc}\mathrm{Tr}[\mathbf{R}'_{oc}[\mathbf{R}' + \mathbf{T}]^{-1}_{cc}\mathbf{R}'_{co}] \tag{23}$$

(note the independence of B on $\mathbf{R}'_{oo}$ expressing the coupling between open channels). All the formal expressions discussed so far may be used with the substitution of the appropriate D_{cc} and B functions. Especially for the resonant widths and provided that (i) and (ii) are valid, the above Multichannel generalization could be applied, in a way complimentary to (or, better, in conjunction with) the R-matrix/MQDT method, for their theoretical prediction.

4 Applications of 4QDT expressions

4.1 The 4d5p^{1}P$_1$ →[5pnp]$_{J=0}$ spectrum of Sr

The even $J = 0$ structure below the Sr $5p_{1/2}$ threshold consists of two interacting closed channels ($[5p_{1/2}np_{1/2}]_{J=0}$ (channel 1) and $[5p_{3/2}np_{3/2}]_{J=0}$ (channel 2)) and three open ones so it is a typical situation where 4QDT can be applied without any loss of information. The spectroscopy and analysis for that spectrum are only preliminary [15]. A detailed presentation is to be given in a forthcoming paper. Part of the experimental spectrum together with the fitted one using 4QDT, around the $[5p_{3/2}13p_{3/2}]_{J=0}$ perturber is shown in Figure 2a. In reference [15] the parameters μ_1, μ_2 and $|R'_{12}|$ were fitted on energy level positions while for the cross-section 3QDT was employed. The appearance of stabilization was avoided by convoluting the spectrum with the laser linewidth (as in Ref. [7]) while saturation effects were also taken into account, implying a small power broadening. Consequently, these data are not very reliable for fitting resonant widths. The accuracy of the obtained parameters is not very high although it is sufficient for testing the 4QDT formulae derived in Section 2. The applicability condition (ii) is valid ($|R'_{12}/R'_{13}R'_{23}| \approx 24$) and so does (iii) at least in the neighborhood of the perturbers. The two closed channels autoionize primarily to different effective continua and therefore any interference effect leading to stabilization is absent. The $\sigma_{max}(E)$ function, shown in Figure 2b, envelopes perfectly the resonant maxima over the whole range of the perturber. However, near the zero minimum of $\sigma_{max}(E)$, occurring outside the perturber, the cross-section is very weak but non-zero (see the inset of Fig. 2b). At this energy range the admixture coefficient of the perturbed series dominates. Hence, the failure of (15) in this range is to be attributed partly to (the ignored) $\sigma^{nr}_{max}(E)$ function and partly to the comparable excitation strength between channel 1 and the continua ((iii) is close to its limit of validity). Despite that, $q(E)$ in (16) (plotted in Fig. 2c) passes smoothly from zero and correctly predicts the occurrence of a q-reversal when $\sigma_{max}(E) = 0$. It is more difficult to identify the second q-reversal because near the pole of $q(E)$ the resonances are symmetric and the reversed asymmetry becomes apparent rather far from that point. In practice, locating the q-reversals provides (together with the use of $\sigma_{max}(E)$) most of the fitted parameters or combinations of them before making any attempt to fit the total cross-section.

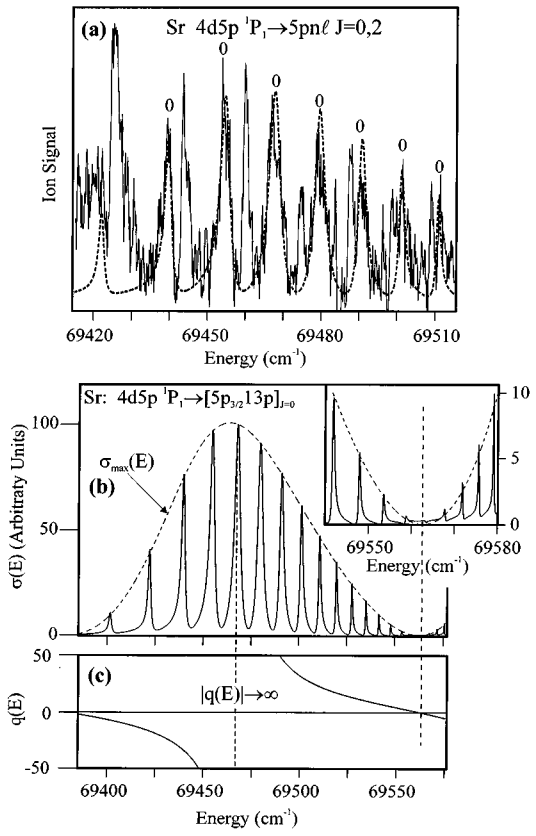

Fig. 2. (a) The Sr $5s^2\ ^1S_0$—$\omega_1 \rightarrow 4d5p\ ^1P_1$—$\omega_2 \rightarrow [5pn\ell]_{J=0,2}$ spectrum (solid line) and fitted $J = 0$ 4QDT spectrum (dashed line), around the $[5p_{3/2}13p_{3/2}]_{J=0}$ perturber with parallel ω_1 and ω_2 polarizations [15]. The $J = 0$ resonances (marked with "0") have been identified through a comparison with spectra recorded with perpendicular polarizations ($[5pn\ell]_{J=1,2}$). (b) The synthetic $J = 0$ total cross-section alone (Eq. (6), full line curve) and $\sigma_{max}(E)$ function (Eq. (15), dashed line curve). Parameters of the preliminary fit based only on the spectrum around the $[5p_{3/2}13p_{3/2}]_{J=0}$ perturber: $Ryd = 109\,736.63$ cm^{-1}, $I_1 = 69\,647.28$ cm^{-1}, $I_2 = 70\,448.74$ cm^{-1}, $\mu_1 = 0.79$, $\mu_2 = 0.42$, $R'_{12} = 0.64$, $R'_{13} = -0.35$, $R'_{23} = 0.1$, $R'_{24} = 0.43$, $d'_1/d'_2 = -0.1$, $d'_3/d'_2 = 0.1$ and $d'_4/d'_2 = -0.02$. The inset shows in an expanded scale the zero minimum region of $\sigma_{max}(E)$. (c) The $q(E)$ function (Eq. (16)). Vertical dashed lines mark the locations of the two q-reversals. The energy scales refer to the Sr ground state.

4.2 The 6snd $^1D_2 \rightarrow$ [6pnd]$_{J=3}$ spectrum of Ba

Using the ICE technique, excitation from the $6snd^1D_2$ bound Rydberg states of Ba revealed two interacting autoionizing series below the $6p_{1/2}$ threshold [11]. These are the $[6p_{1/2}nd_{5/2}]_{J=3}$ (channel 1) and the $[6p_{3/2}nd^+]_{J=3}$ (channel 2) where nd^+ denotes the linear combination $\sqrt{2/5}nd_{3/2} + \sqrt{3/5}nd_{5/2}$ [12]. Another series, the $[6p_{3/2}nd^-]_{J=3}$, does not significantly interact with the other two and is not efficiently excited from the $6snd^1D_2$ states. Thus, 4QDT is appropriate for the analysis of this spectrum. The spectral profiles were fitted using one and two open channels models [11] within the eigenchannel MQDT formulation [17], the Phase-Shifted 3QDT [7] and a six channel Phase-Shifted QDT including all the $[6pnd]_{J=3}$ series and three continua [12]. The 3QDT model reproduced many of the spectral characteristics but it predicted the appearance of stabilization which is absent in the experimental data. The six channel Phase-Shifted QDT fit was quite satisfactory. Nevertheless, the remarkable variation of the widths of the $[6p_{1/2}nd]_{J=3}$ resonances, observed near the $[6p_{3/2}nd^+]_{J=3}$ perturbers was basically analyzed qualitatively. It is especially this variation that we would like to reproduce by fitting the experimental data using (14).

In a step by step procedure, $|R'_{12}|$, μ_1 and μ_2 are first determined by an analysis of energy level positions [7,11]. The remaining parameters R'_{13}, R'_{23} ($|R'_{12}/R'_{13}R'_{23}| \approx 13$) and R'_{24} as well as the relative sign of all the coupling parameters are then determined by a fit on the resonant widths, using (14). The function $\Gamma(E)$ is shown in Figure 3a. It is nicely reproducing the behavior of the experimental widths even far from the perturbers where the 3QDT curve [7] (see Fig. 3a), obviously fails. The reason for this disagreement is that the two closed channels autoionize primarily to different continua, supporting the simplifying assumption made in the six channel fit that each closed channel is coupled to a single continuum [12]. The points marked with white boxes correspond to the resonances at 61 171.7 cm^{-1} and 61 901.0 cm^{-1}, assigned to the $[6p_{3/2}9d^+]_{J=3}$ and $[6p_{3/2}10d^+]_{J=3}$ states respectively [11]. Experimental widths were not provided for those lines because they completely disagree (much smaller) with those expected on the basis of unperturbed Rydberg series. These levels are strongly mixed with the perturber which extends over a much broader energy range. The experimental ICE cross-section around the $[6p_{3/2}10d^+]_{J=3}$ perturber (Fig. 3b) is satisfactorily reproduced in Figure 3c despite the fact that it is not fitted directly. All the parameters are determined by fitting energy level positions and widths separately. The non-zero background between successive resonances results from the specific relative signs among the coupling parameters upon which the width variation depends critically. This demonstrates the usefulness of (14) in the analysis of complex resonances since the widths are very sensitive probes of channels interactions. Finally, $q^{ICE}(E)$ in Figure 3d reveals a q-reversal which indeed shows up in the spectrum.

4.3 The $3d^94s(^1D_2)$ nd $^2G_{9/2} \leftrightarrow 3d^94p^2\ ^4F_{9/2}$ interaction in Cu: applicability investigation

Below the Cu II $3d^94s(^{3,1}D)$ thresholds, the interaction between the $3d^94s(^1D_2)nd\ ^2G_{9/2}$ series (channel 1) with the $3d^94p^2\ ^4F_{9/2}$ state (belonging to channel 2), excited from the metastable $3d^94s4p\ ^4F_{9/2}$ states, results in a particularly complex spectrum. The latter is shown in Figure 4a together with a fit using a Phase-Shifted MQDT model composed of two closed and two open channels [16]. All the possible coupling parameters were initially included. Based on a complementary Hartree-Fock (HF)

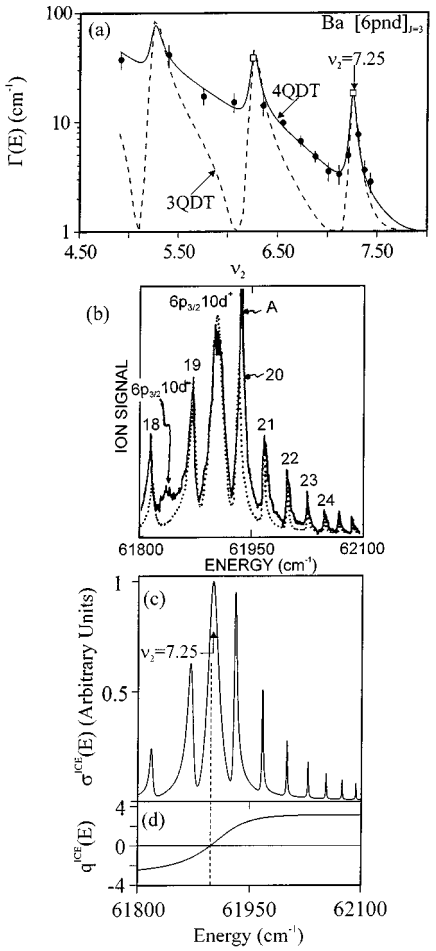

Fig. 3. ICE $6snd\ ^1D_2 \rightarrow [6pnd]_{J=3}$ spectrum of Ba. Parameters of the fit: $Ryd = 109\,736.87$ cm^{-1}, $I_1 = 62\,296.49$ cm^{-1}, $I_2 = 63\,987.35$ cm^{-1}, $\mu_1 = 0.80$, $\mu_2 = 0.75$, $R'_{12} = 0.26$, $R'_{13} = 0.29$, $R'_{23} = 0.07$ and $R'_{24} = 0.29$. (a) The functions $\Gamma(E)$ for 4QDT (full line, Eq. (14)) and 3QDT [7] (dashed line), *versus* the effective quantum number ν_2. The functions are convoluted to the 1 cm^{-1} laser linewidth. Black points denote the experimental data of reference [11]. For the white boxes see text. (b) Experimental $6s10d\ ^1D_2 \rightarrow [6p_{3/2}10d^+]_{J=3}$ spectrum (full line) and six channel QDT fit (dotted line) [12]. The line marked with "A" is a parasitic one, masking the "$[6p_{1/2}20d]_{J=3}$" resonance. (c) Synthetic ICE cross-section using the above 4QDT parameters. (d) The $q^{ICE}(E)$ function, equation (21). The predicted q-reversal is shown with the dashed vertical line. The energy scale refers to the Ba ground state.

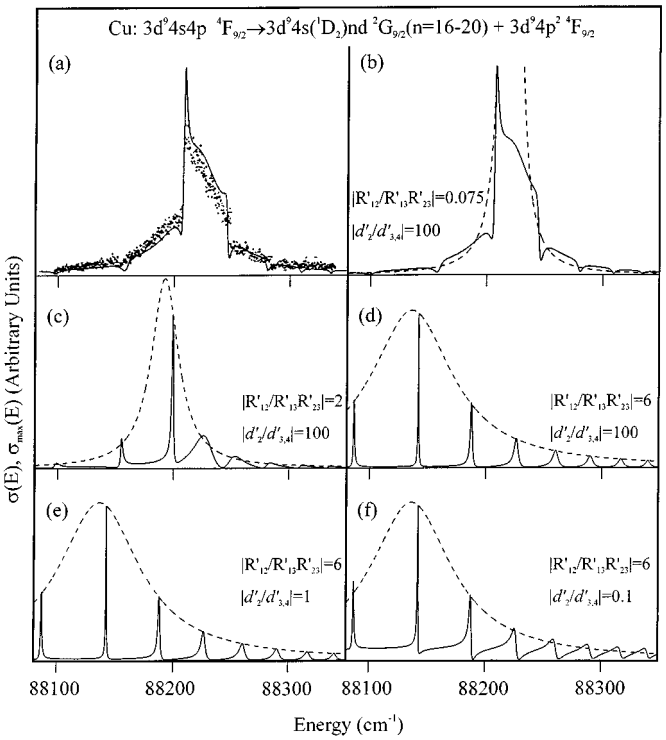

Fig. 4. (a) Experimental $3d^9 4s4p\ ^4F_{9/2} \rightarrow 3d^9 4s(^1D_2)nd\ ^2G_{9/2} + 3d^9 4p^2\ ^4F_{9/2}$ spectrum of Cu (points) and fitted MQDT profile (solid line) [16]. (b) The present 4QDT fit with the following parameters: $Ryd = 109\,736.37$ cm^{-1}, $I_1 = 88\,581.0$ cm^{-1}, $I_2 = 128\,735.9$ cm^{-1}, $\mu_1 = 0.896$, $\mu_2 = 0.354$, $R'_{12} = 0.001$, $R'_{13} = -0.5$, $R'_{23} = 0.03$, $R'_{24} = 0.017$, $d'_1/d'_2 = 0.01$, $d'_3/d'_2 = 0.01$, $d'_4/d'_2 = 0.01$. Dashed line curves denote the $\sigma_{max}(E)$ function, equation (15). (c) Same as in (b) but with $R'_{12} = 0.03$. (d) Same as in (b) but with $R'_{12} = 0.09$. (e) and (f) same as in (d) but with $d'_3/d'_2 = d'_4/d'_2 = 1$ and 10 respectively. The energy scale refers to the the Cu ground state.

analysis, many of them were subsequently set equal to zero. In Figure 4b is shown the spectrum fitted using the 4QDT model of Figure 1. Because some non-zero couplings of the model of reference [16] are not included in 4QDT and because the two synthetic spectra are not completely identical, a somewhat different set of parameters emerged. As expected, however, the important conclusions of the present analysis agree with those in [16]. Most striking is the fact that the closed channels interact essentially through the continua ($|R'_{12}/R'_{13}R'_{23}| \approx 0.075$), their direct interaction being negligible. As a consequence condition (ii) is invalid (while (iii) still holds) and $\sigma_{max}(E)$, $\Gamma(E)$ and $q(E)$ should not describe the observed spectrum. This is illustrated in Figure 4b where $\sigma_{max}(E)$ fails to envelope properly the cross-section. Thus, this spectrum may serve as the starting point of an investigation leading to quantitative applicability limits for the expressions derived in Section 2. First, the direct closed channel coupling R'_{12} is gradually increased until $\sigma_{max}(E)$ properly predicts the line intensities. Characteristic examples are shown in Figure 4c (for $|R'_{12}/R'_{13}R'_{23}| = 2$) and in Figure 4d (for $|R'_{12}/R'_{13}R'_{23}| = 6$). In the former case a considerable improvement can be observed while the latter represents the lowest value for which the description of the line intensities is excellent. Therefore, for the 4QDT case, an empirical rule for condition (ii) to be fulfilled is

$$|R'_{12}/R'_{13}R'_{23}| \geq 6. \tag{24}$$

Similar rules may be constructed for more complex models. It is emphasized that if (24) is not fulfilled the envelope

will not be predicted even if the approximation (12) is not applied and (11) is used instead.

In Figure 4c the ratios $|d'_2/d'_{3,4}| = 100$ validate (iii) close to the perturber. However, even far from the latter, $\sigma_{max}(E)$ does predict correctly the line maxima, despite the fact that $|d'_1/d'_{3,4}| = 1$. Its behavior is examined by increasing the matrix elements $d'_{3,4}$ (see the examples in Figs. 4e–f). The emerging applicability limit for (15) and (16) appears to be

$$|d'_2/d'_{3,4}| \geq 1. \tag{25}$$

Rather surprisingly, for $|d'_2/d'_{3,4}| < 1$ $\sigma_{max}(E)$ proves to be inapplicable even by using (11) instead of (12) (including the contribution of ϵ_{nr}). Hence, it is *a posteriori* revealed that even for (11) to be meaningful, (iii) must be valid. In that case however, (12) is a very good approximation and much simpler.

5 Summary and conclusion

A method for obtaining approximate formulae for the energy dependence of spectral line intensities, asymmetries and autoionization widths, for MQDT models with two effective open channels, was presented. It relies in attributing the resonant behavior to only one of the solutions of the compatibility equation, related to the common phase shifts of the two open channels. The aforementioned quantities are then calculated using only this resonant solution and by applying the well-known procedures as for the simpler single-continuum problem. Irrespectively of the number of open channels, the latter procedures are applicable only when rather restrictive conditions are fulfilled. Those conditions of applicability, discussed so far only fragmentarily in the literature, were presented here in detail. The method provides analytical expressions for a model consisting of two interacting closed channels converging towards different ionization limits and coupled to two effective continua. These analytical formulae, representing the extensions of those previously derived for the corresponding model with one open channel, were tested on experimental spectra of Sr, Ba and Cu. Furthermore, it was shown that a generalization of the method for an arbitrary number of continua is possible. However, for a large number of interacting channels analytical expressions are difficult to find and the usefulness of parametric MQDT models is rather limited. In this case the derived formal, many-open-channel expressions may be used complementarily and in conjunction with R-matrix/MQDT treatments.

The author is grateful to P. Camus, M. Aymar, J. M. Lecomte and A. Lyras for reading the manuscript and for their valuable suggestions and comments.

References

1. M.J. Seaton, Rep. Prog. Phys. **46**, 167 (1983).
2. M. Aymar, C.H. Greene, E. Luc-Koening, Rev. Mod. Phys. **68**, 1015 (1996) and references therein.
3. A. Giusti-Suzor, U. Fano, J. Phys. B **17**, 215 (1984).
4. W.E. Cooke, C.L. Cromer, Phys. Rev. A **32**, 2725 (1985).
5. U. Fano, Phys. Rev. A **124**, 1866 (1961).
6. J.M. Lecomte, J. Phys. B **20**, 3645 (1987).
7. A. Gusti-Suzor, H. Lefebvre-Brion, Phys. Rev. A **30**, 3057 (1984).
8. H. Friedrich, D. Wintgen, Phys. Rev. A **32**, 3231 (1985).
9. H. Friedrich, D. Wintgen, Phys. Rev. A **31**, 3964 (1985).
10. D. Wintgen, H. Friedrich, Phys. Rev. A **35**, 1628 (1987).
11. F. Gounand, T.F. Gallagher, W. Sandner, K.A. Safinya, R. Kachru, Phys. Rev. A **27**, 1925 (1983).
12. O.C. Mullins, Y. Zhu, E.Y. Xu, T.F. Gallagher, Phys. Rev. A **32**, 2234 (1985).
13. J.P. Connerade, A.M. Lane, M.A. Baig, J. Phys. B **18**, 3507 (1985).
14. H. Hieronymus, J. Neukammer, H. Rinneberg, J. Phys. B **25**, 3463 (1992).
15. M. Kompitsas, in *Proceedings of the 7th International School on Quantum Electronics/Lasers-Physics and Applications, Sofia, Bulgaria 1992*, edited by P.A. Atanasov (Institute of Electronics, Bulgarian Academy of Sciences, 1992), p. 113.
16. M. Martins, P. Zimmermann, Z. Phys. D **27**, 115 (1993).
17. K.T. Lu, U. Fano, Phys. Rev. A **2**, 81 (1970); U. Fano, Phys. Rev. A **2**, 353 (1970); C.M. Lee, K.T. Lu, Phys. Rev. A **8**, 1241 (1973).
18. H. Friedrich, *Theoretical Atomic Physics* (Springer, New York, 1990), p. 154.
19. W.H. Press, S.A. Teukolsky, W.T. Vetterling, B.P. Flannery, *Numerical Recipes*, 2nd edn. (Cambridge University Press, Cambridge, 1992).
20. K. Ueda, Phys. Rev. A **35**, 2484 (1987).
21. Q. Wang, C.H. Greene, Phys. Rev. A **44**, 1874 (1991).
22. S.A. Bhatti, C.L. Cromer, W.E. Cooke, Phys. Rev. A **24**, 161 (1981).